Scripta Materialia 165 (2019) 73–77

Contents lists available at ScienceDirect

Scripta Materialia

journal homepage: www.elsevier.com/locate/scriptamat

# Diffusion kinetics in binary CuZr and NiZr alloys in the super-cooled liquid and glass states studied by nanocalorimetry

Dongwoo Lee [a], Joost J. Vlassak [b,*]

[a] School of Mechanical Engineering, Sungkyunkwan University, Suwon, Gyeonggi-do 16419, South Korea
[b] School of Engineering and Applied Sciences, Harvard University, Cambridge, MA 02138, United States

ARTICLE INFO

*Article history:*
Received 7 January 2019
Received in revised form 9 February 2019
Accepted 9 February 2019
Available online xxxx

*Keywords:*
Metallic glass
Diffusion
Solid state
Super-cooled liquid
Nanocalorimetry

ABSTRACT

In this work, we use nanocalorimetry to characterize the diffusion kinetics of Cu-Zr and Ni-Zr glass-forming alloys in both the solid state and the super-cooled liquid state, covering a temperature range from $0.67T_g$ to $1.49T_g$. We find that diffusion in the solid state follows Arrhenius behavior, while the kinetics in the super-cooled liquid state is well described by a fragility-based model that takes into account breakdown of the Stokes-Einstein relationship between the diffusivity and viscosity. The current work uses a single experimental technique to map out the kinetics of diffusion over a broad temperature range in both states.



Metallic glasses (MG) are a class of alloys that command great interest because they combine metallic properties with the ease of molding of polymers [1–3]. Since crystallization needs to be suppressed both during cooling from the melt and during processing, design of MG requires detailed understanding of the transport properties in these alloys, both in the solid state (SS) and in the super-cooled liquid state (SLS). Measurement of diffusion kinetics over a wide range of temperatures covering both SS and SLS with a single technique is difficult. Furthermore, glass forming alloys with poor thermal stability, such as binary metallic systems, do not provide sufficient times scales for conventional experiments: Even for alloy systems with very high glass-forming ability (GFA), measurement of diffusion kinetics above $1.1T_g$ is not possible due to crystallization [4]. Consequently, experimental results on the diffusion kinetics in binary glass-forming systems in a wide temperature range in SS and SLS are scarce.

A number of techniques have been used to study diffusion kinetics in metallic systems, including secondary ion mass spectroscopy (SIMS), Auger electron spectroscopy (AES), nuclear-reaction analysis, and calorimetry [5–8]. Most techniques used thus far work only over a relatively small temperature range or have other restrictions that make them not generally applicable. Here, we use nanocalorimetry to investigate the diffusion kinetics in binary Cu-Zr and Ni-Zr glass-forming alloys, over a temperature range that covers both the solid state and the super-cooled liquid state. The dynamic range of the technique makes it possible to access a temperature range of $0.67T_g$ to $1.49T_g$, corresponding to heating rates from approximately 10 K/s to $10^5$ K/s [9–11].

In this study, the diffusion kinetics in the SS is evaluated for the CuZr and NiZr systems by preparing polycrystalline multilayers that form a metallic glass upon intermixing. The activation energy of diffusion is readily determined from the calorimetry measurements. The diffusion kinetics in the SLS is evaluated indirectly by measuring the crystallization kinetics of the alloys over a range of temperatures. Crystallization, rather than being an obstacle to the study of super-cooled liquids, presents an important window onto their structural relaxation [12]. Calorimetry measurements performed at different heating rates provide information on the kinetics of crystallization, which may be analyzed in terms of atomic transport.

For the experiments described in this study, four different types of samples were prepared: 500 nm films of both $Cu_{50}Zr_{50}$ ($102 \pm 10$ nmol) and $Ni_{50}Zr_{50}$ ($106 \pm 10$ nmol) metallic glasses (MGs), and 100 nm multilayers (MLs) of both Cu/Zr ($20 \pm 2$ nmol) and Ni/Zr ($21 \pm 2$ nmol). The multilayers had a bilayer period of 25 nm and overall stoichiometry of $X_{50}Zr_{50}$, where X represents either Cu or Ni. The samples were characterized using nanocalorimetry, a technique where micromachined sensors are used to perform very sensitive calorimetry measurements on thin films. Details of the nanocalorimetry technique, deposition parameters for the films, characterization methods can be found in the Supplementary Information.

Fig. 1a shows the heat flow for a Ni/Zr multilayer sample obtained from a nano–calorimetry measurement. A broad exothermic reaction is observed, starting at approximately 480 K and peaking at 735 K. This peak is followed by a smaller peak at 815 K. The total enthalpy

* Corresponding author.
*E-mail address:* vlassak@seas.harvard.edu (J.J. Vlassak).

https://doi.org/10.1016/j.scriptamat.2019.02.014
1359-6462/

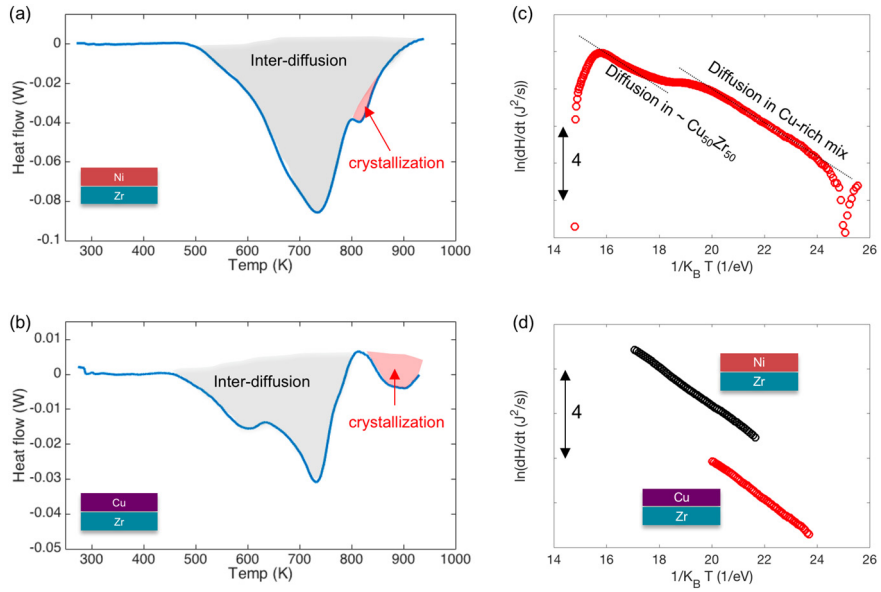


**Fig. 1.** Heat flow vs. temperature curves of (a) Ni/Zr and (b) Cu/Zr multilayers. Both systems have a total thickness of 100 nm and a bilayer period of 25 nm. The average heating rate of the nanocalorimetry measurements were 15,000 K/s. (c) Arrhenius graph of the inter-diffusion in the Cu/Zr multilayer; (d) Inter-diffusion in both Cu/Zr and Ni/Zr multilayers have an activation energy of approximately 1.0 eV.

associated with the Ni/Zr reaction was calculated by integrating the heat flow with respect to time and was found to be $-23.3 \pm 3$ kJ/mol. This value is similar to the amorphization enthalpy of 28 kJ/mol of a NiZr multilayer with overall composition of $Ni_{56}Zr_{44}$ and a wavelength of 74 nm [13]. The reaction behavior of Ni/Zr multilayers has been studied previously using various techniques, including differential scanning calorimetry (DSC) and X-ray diffraction (XRD) [13–17]. It was shown that the low- and high-temperature reactions correspond to diffusion-controlled amorphization and crystallization, respectively.

Fig. 1b depicts the heat flow for a typical Cu/Zr multilayer sample. It is evident from the figure that the reaction in the Cu/Zr multilayer proceeds in three reaction stages, with significant overlap between the first two stages. The peak temperatures for each reaction are 605, 730, and 900 K, respectively. X-ray diffraction measurements of Cu/Zr multilayers that were quenched at different reaction stages confirmed that the initial multilayer structure consists of crystalline Zr (hcp) and Cu (fcc), which have {002} and {111} crystallographic textures, respectively (Supplementary Information). As the reaction proceeds, the Cu peak disappears first, followed by the Zr peak, until finally no more diffraction peaks associated with the sample can be observed. These observations indicate that the Cu layer is consumed first as an amorphous phase forms at the original Cu/Zr interfaces. Since the radius of the Cu (128 pm) atom is much smaller than the Zr atom (160 pm), one would expect diffusion of Cu into the amorphous matrix to be faster than Zr, leading to the formation of a Cu-rich amorphous matrix in the first stage of the reaction. As the rest of the Zr is consumed, the amorphous phase eventually becomes equiatomic, resulting in the second exotherm (Supplementary Information). The amorphous CuZr matrix then crystallizes to form $CuZr_2$ and $Cu_{10}Zr_7$ in the third stage. Similar to the Ni/Zr system, the Cu/Zr multilayer has a large exothermic peak due to inter-diffusion, followed by a much smaller crystallization peak. The enthalpy of inter-diffusion was measured to be $12 \pm 2$ kJ/mol, while the crystallization enthalpy was 2.7 kJ/mol.

Highmore et al. [13,18] have shown that the enthalpy produced during inter-diffusion obeys the following equation [13].

$$\ln\left(H\frac{dH}{dt}\right) = \ln(H_O) - \frac{Q^{SS}}{k_B T}. \quad (1)$$

Here, $H$ is the enthalpy produced during the amorphization process and $H_o$ is a constant. According to Eq. (1), the activation energy of inter-diffusion $Q^{SS}$ can be determined from the slope of the $\ln(HdH/dt)$ vs. $1/k_BT$ curve. Fig. 1c shows an Arrhenius graph for a Cu/Zr multilayer sample. For the temperature range associated with the first and the second inter-diffusion processes, the slope is constant, indicating that the amorphization kinetics is indeed diffusion-limited for the Cu/Zr system. As mentioned earlier, the low-temperature diffusion process is associated with the formation of a Cu-rich Cu/Zr amorphous phase as a result of Cu diffusion, while the high-temperature process corresponds to the formation of the equiatomic amorphous phase as a result of continued Zr diffusion into the amorphous phase. Interestingly, the change in composition of the amorphous phase does not change the activation energy of the inter-diffusion process in the Cu/Zr system, at least not within experimental error – both processes have an activation energy $Q^{SS}$ of $1.0 \pm 0.07$ eV. Fig. 1d compares the Arrhenius graph of the first inter-diffusion process in the Cu/Zr multilayer system with that for the Ni/Zr system. Similar to the Cu/Zr system, the curve of the Ni/Zr system produces a curve with a constant slope, and the corresponding activation energy is $0.95 \pm 0.07$ eV, which is slightly smaller than the previously reported value of 1.1 eV [13]. The nanocalorimetry results indicate that diffusion in the Cu/Zr and Ni/Zr systems is thermally activated in the glassy state.

Fig. 2a and b shows the heating rates versus temperature obtained from nanocalorimetry measurements on amorphous $Cu_{50}Zr_{50}$ and $Ni_{50}Zr_{50}$ samples. These curves show signals corresponding to the glass transition and crystallization process. Crystallization peaks are indicated in the figures. For both material systems, the crystallization temperatures increase with heating rate. The peak crystallization temperatures and corresponding heating rates can be used to construct Kissinger plots as shown in Fig. 2c [19–23], the slope of which is the activation energy of crystallization. In addition to the nanocalorimetry measurements, which cover a range of heating rates from 10 to $10^5$ K/s, we also show a few data points obtained from the literature to further expand the temperature range of the analysis. The literature data were obtained using conventional calorimetry with heating rates varying from 0.17 to 1.00 K/s [24–27]. It is evident from Fig. 2c that the slope, which represents the activation energy of the crystallization process, gradually reduces as the temperature increases. This behavior

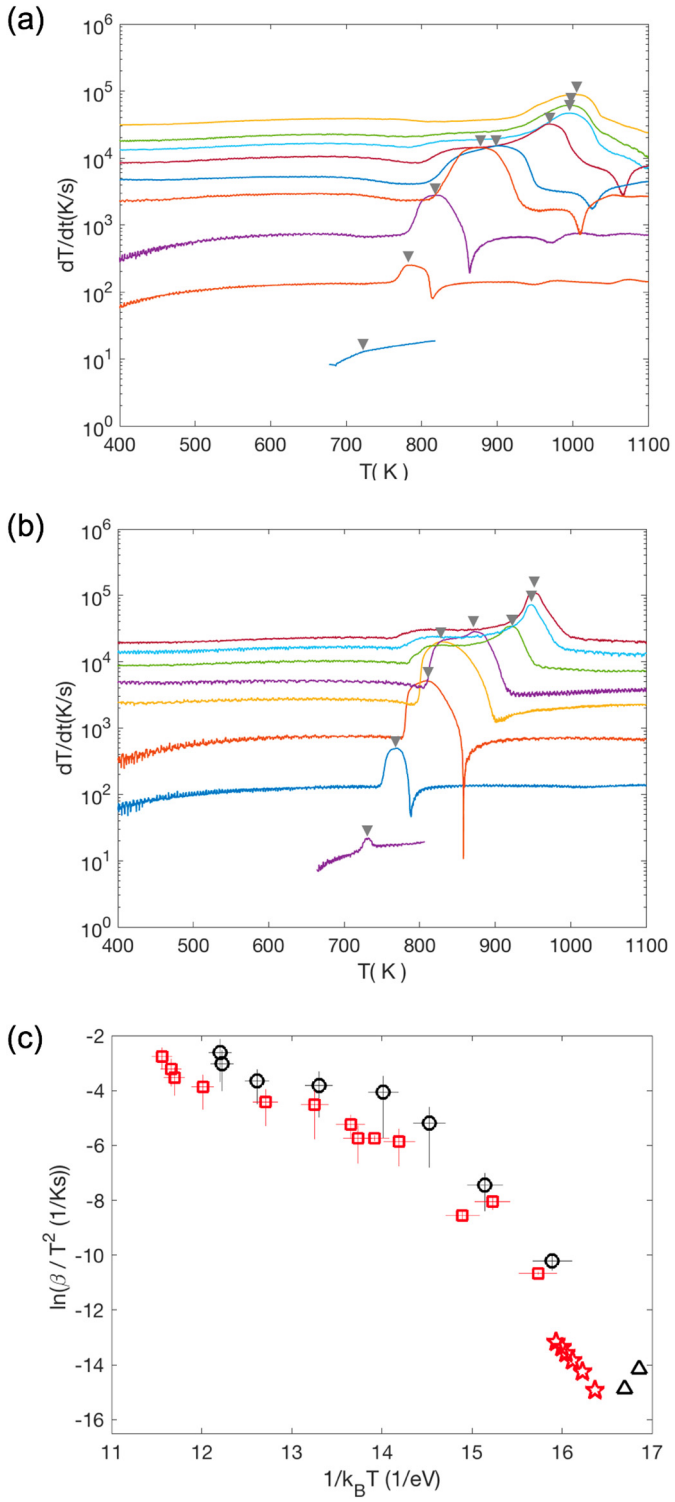


**Fig. 2.** (a) Heating rate vs. temperature of $Cu_{50}Zr_{50}$ metallic glasses – crystallization peaks are marked. (b) heating rate vs. temperature curves of $Ni_{50}Zr_{50}$ metallic glasses. (c) Kissinger plot of the crystallization kinetics of $Cu_{50}Zr_{50}$ (red) and $Ni_{50}Zr_{50}$ (black) metallic glasses. Square ($Cu_{50}Zr_{50}$) and circular ($Ni_{50}Zr_{50}$) data points were acquired from the nanocalorimetry measurements in this work, while star ($Cu_{50}Zr_{50}$) and triangular ($Ni_{50}Zr_{50}$) points are from literature [24–27]. (For interpretation of the references to color in this figure legend, the reader is referred to the web version of this article.)

is fundamentally different from the inter-diffusion processes observed in the multilayer samples, which do follow Arrhenius kinetics with a constant activation energy.

The temperature-dependence of the crystallization activation energies shown in Fig. 2c can be described by considering the crystal growth rate, $u$, given by [28]

$$u(T) = u_{kin}\left[1 - exp\left(-\frac{\Delta G(T)}{k_B T}\right)\right]. \quad (2)$$

Here $\Delta G(T)$ is the free energy difference between the super-cooled liquid and the crystalline phases, which can be approximated as $2T\Delta H_f(T_m - T)/[T_m(T_m + T)]$, where $T_m$ is the melting temperature [29]. $u_{kin}$ is the kinetic growth rate which scales with diffusivity of the super-cooled liquid, and the other symbols have their usual meanings. The temperature-dependence of $u_{kin}$ is well described by a phenomenological model based on the viscosity and fragility of the super-cooled liquid state if a result obtained by Ediger et al. [28] is invoked. In the super-cooled regime, the well-known Stokes-Einstein relationship between viscosity and diffusivity breaks down and is replaced by a power-law relation of the form, $D^{SLS} \propto \eta^{-\xi}$, where $\eta$ is the viscosity of the super-cooled liquid. [19,30]. The decoupling exponent $\xi$ can be estimated as $\xi \approx 1.1 - 0.005m$, where $m$ is the fragility of the super-cooled liquid. The viscosity data were obtained from the literature [24,31–33] and were fitted with the Vogel-Fulcher-Tammann (VFT) equation, $\eta(T) = \eta_o \exp(\frac{D^* T_o}{T - T_o})$, yielding the fragility values of 99 and 133 for the $Cu_{50}Zr_{50}$ and $Ni_{50}Zr_{50}$ system, and decoupling exponents $\xi$ of 0.60 and 0.44 for the two systems, respectively (Supplementary Information). The VFT equation combined with the Ediger result yields the following expression for the kinetic growth rate

$$u_{kin}(T) = C\eta(T)^{-\xi}. \quad (3)$$

Using Eq. (2), the Kissinger plots of the crystallization processes in Fig. 2c can be converted into Arrhenius graphs of $u_{kin}$, or equivalently, the diffusivity in the SLS ($D^{SLS}$) as shown in Fig. 3a. Eq. (3) is shown in the same graph along with the experimental data. The proportionality constant, $C$, in the equation was selected to translate the curves vertically to match the experimental data. It is evident that this simple phenomenological model describes the experimental temperature dependence of $u_{kin}$ quite well.

The slopes of the Arrhenius graphs, which are the apparent activation energies of transport in the super-cooled liquid states ($Q^{SLS}$), are shown in Fig. 3b as a function of $1/k_BT$. While $Q^{SLS}$ is not a real activation energy, its value does provide a measure of how transport in a material system changes with temperature. It is clear from the figure that the value of $Q^{SLS}$ at a given temperature is similar for both material systems. However, the glass forming ability of an alloy depends sensitively on both the glass transition and liquidus temperatures [34]. Consequently, it makes sense to scale the temperature accordingly. Fig. 3c shows the value of $Q^{SLS}$ as a function of $\Delta T_{norm} = (T_m - T)/(T_m - T_g)$. It is evident that the value of $Q^{SLS}$ for $Cu_{50}Zr_{50}$ is always higher than that for $Ni_{50}Zr_{50}$ at the same relative level of undercooling. This observation implies that on cooling transport slows down faster in $Cu_{50}Zr_{50}$ than in $Ni_{50}Zr_{50}$ at the same relative level of undercooling. Furthermore, the liquidus temperature $T_m$ is much closer to the glass transition temperature for $Cu_{50}Zr_{50}$ than for $Ni_{50}Zr_{50}$, i.e., the change in transport kinetics occurs over a much narrower temperature range. This observation suggests that the former has better glass forming ability, consistent with previous findings [25,35,36], and that the following dimensionless quantity

$$\Xi = \frac{Q^{SLS}}{k_B(T_m - T_g)}, \quad (4)$$

depicted as a function of relative undercooling in Fig. 3d, may be a good measure for the glass forming ability of an alloy. Since $Q^{SLS}$ depends sensitively on the fragility, Eq. (4) demonstrates that the glass-forming ability of a metallic glass depends on $T_g$, $T_m$ and the fragility. This observation is in good agreement with recent work by Johnson et al.

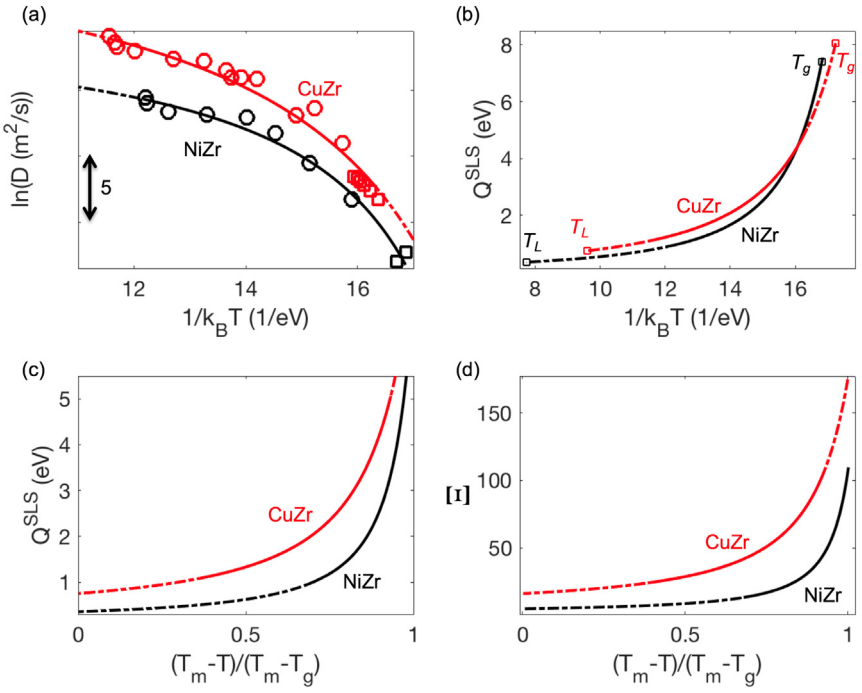


**Fig. 3.** (a) Arrhenius plot of $D^{SLS}$ from the calorimetry results (markers) and Eq. (3) (lines). Apparent activation energies for $Cu_{50}Zr_{50}$ (red) and $Ni_{50}Zr_{50}$ (black) systems, with respect to (b) $1/k_BT$ and (c) $\Delta T_{norm}$. (d) Ξ versus $\Delta T_{norm}$. Solid lines correspond to temperature ranges with experimental data, while dashed lines are extrapolations using the fragility-based model. (For interpretation of the references to color in this figure legend, the reader is referred to the web version of this article.)

[34], who have shown that the critical thickness of glass-forming alloys can be described by a simple expression containing the fragility and the reduced temperature, $T_g/T_L$.

Following the discussion in the previous sections, the diffusivity in the SS and SLS can be described using the following expressions,

$$D^{SS} = D_o^{SS} \exp\left(-\frac{Q^{SS}}{k_B T}\right), \tag{5}$$

$$D^{SLS} = C\left(\eta_o \exp\left(\frac{D^* T_o}{T - T_o}\right)\right)^{-\xi}, \tag{7}$$

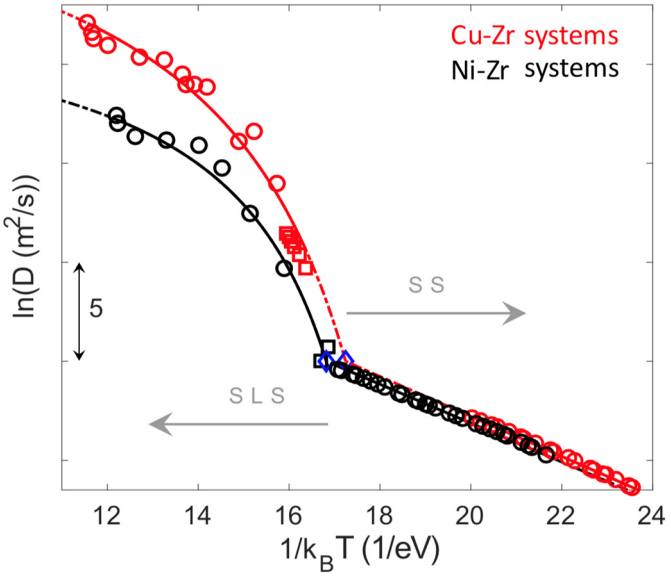


**Fig. 4.** Diffusion kinetics of CuZr and NiZr in SLS and SS region obtained from the calorimetry measurements.

respectively. Fig. 4 shows an Arrhenius graph of the diffusivity of $Cu_{50}Zr_{50}$ and $Ni_{50}Zr_{50}$ over a temperature range covering both SLS and SS. The pre-exponential factor in Eq. (5) was determined from the requirement that the diffusivity be continuous at $T_g$. It is clear that the glass transition causes an abrupt increase in the slope of the diffusivity graphs. This behavior is also observed in molecular dynamics simulations of diffusion in molten and glassy NiZr [37,38] and $Cu_{33}Zr_{67}$ [39]. Several models have been proposed to explain the enhanced mobility in the SLS. One model attributes the higher apparent activation energy above the glass transition temperature to structural changes in the matrix on a timescale comparable to the interval between individual atomic hopping events. These structural changes would enhance the hopping probability and lead to increased diffusion [4]. More recently, it was shown experimentally that the enhanced diffusivity above the glass transition is not due to an increase in single-atom hopping rate, which follows Arrhenius behavior with the same activation energy in both states. Instead, it is the result of a collective process, in which a small group of atoms in the SLS move in a highly coordinated fashion [40]. We hope that experimental data such as the data presented in this paper will prove useful in developing quantitative models for atomic transport in metallic glasses.

In conclusion, we have utilized nanocalorimetry sensor arrays to characterize the diffusion behavior in the solid states and the supercooled liquid states of NiZr and CuZr, covering a wide range of temperatures from $0.67T_g$ to $1.49T_g$, which may not be accessible with a single conventional experimental technique. The diffusion behavior in the solid state is investigated by characterizing the inter-diffusion and amorphization of elemental multilayers; diffusion behavior in the super-cooled liquid state is analyzed by studying the crystallization kinetics of amorphous samples. We demonstrate that diffusion in the solid state is controlled by a single value of the activation energy in a typical Arrhenius process. Diffusion in the super-cooled liquid state is highly non-Arrhenius with an apparent activation energy that deceases rapidly as the temperature increases above the glass transition. This behavior is well described using a phenomenological model relating the diffusivity to viscosity and the fragility of the super-cooled liquid state. We believe that the nanocalorimetry technique introduced in this

paper may be used to study diffusion kinetics in binary systems that form amorphous phases on sputter deposition, over a temperature range covering both the SS and SLS.

## Declarations of interest

None.

## Acknowledgements

This work was supported by the National Science Foundation under Grant DMR-1435820 and by the Air Force Office of Scientific Research under Grant FA9550-16-1-0180 (Aerospace Materials for Extreme Environments Program). It was performed in part at the Center for Nanoscale Systems at Harvard University, which is supported by the National Science Foundation under Award No. ECS-0335765, and at the Materials Research Science and Engineering Center at Harvard University, which is supported by the National Science Foundation under Award No. DMR-14-20570. D Lee acknowledges the support from Basic Science Research Program through the National Research Foundation of Korea (NRF) funded by the Ministry of Science, ICT and Future Planning (NRF-2017M1A7A1A01016221 and 2017R1E1A1A01078324).

## Supplementary information

Supplementary information to this article can be found online at https://doi.org/10.1016/j.scriptamat.2019.02.014.

## References

[1] M.F. Ashby, A.L. Greer, Scr. Mater. 54 (3) (2006) 321–326.
[2] G. Kumar, A. Desai, J. Schroers, Adv. Mater. 23 (4) (2011) 461–476.
[3] J. Schroers, Phys. Today 66 (2) (2013) 32–37.
[4] U. Geyer, S. Schneider, W.L. Johnson, Y. Qiu, T.A. Tombrello, M.P. Macht, Phys. Rev. Lett. 75 (12) (1995) 2364–2367.
[5] F. Faupel, W. Frank, M.P. Macht, H. Mehrer, N. V, K. Ratzke, H.R. Schober, S.K. Sharma, H. Teichler, Rev. Mod. Phys. 75 (1) (2003) 237–280.
[6] D. Holland-Moritz, S. Stüber, H. Hartmann, T. Unruh, T. Hansen, A. Meyer, Phys. Rev. B 79 (6) (2009), 064204. .
[7] C. Michaelsen, K. Barmak, T.P. Weihs, J. Phys. D. Appl. Phys. 30 (23) (1997) 3167–3186.
[8] S.W. Basuki, F. Yang, E. Gill, K. Rätzke, A. Meyer, F. Faupel, Phys. Rev. B 95 (2) (2017), 024301. .
[9] E.A. Olson, M. Yu, Y. Efremov, M. Zhang, Z.S. Zhang, L.H. Allen, J. Microelectromech. Syst. 12 (3) (2003) 355–364.
[10] K.C. Xiao, J.M. Gregoire, P.J. McCluskey, J.J. Vlassak, Rev. Sci. Instrum. 83 (11) (2012), 114901. .
[11] E. Zhuravlev, C. Schick, Thermochim. Acta 505 (1–2) (2010) 1–13.
[12] M.D. Ediger, Annu. Rev. Phys. Chem. 51 (2000) 99–128.
[13] R.J. Highmore, J.E. Evetts, A.L. Greer, R.E. Somekh, Appl. Phys. Lett. 50 (10) (1987) 566–568.
[14] B.M. Clemens, W.L. Johnson, R.B. Schwarz, J. Non-Cryst. Solids 61-62 (1984) 817–822.
[15] B.M. Clemens, Phys. Rev. B 33 (11) (1986) 7615–7624.
[16] Y.T. Cheng, W.L. Johnson, M.A. Nicolet, Appl. Phys. Lett. 47 (8) (1985) 800–802.
[17] J.C. Barbour, Phys. Rev. Lett. 55 (26) (1985) 2872–2875.
[18] R.J. Highmore, R.E. Somekh, J.E. Evetts, A.L. Greer, J. Less-Common Met. 140 (1988) 353–360.
[19] D.W. Lee, B.G. Zhao, E. Perim, H.T. Zhang, P. Gong, Y.L. Gao, Y.H. Liu, C. Toher, S. Curtarolo, J. Schroers, J.J. Vlassak, Acta Mater. 121 (2016) 68–77.
[20] D. Lee, G.D. Sim, K.C. Xiao, J.J. Vlassak, J. Phys. Chem. C 118 (36) (2014) 21192–21198.
[21] D. Lee, G.D. Sim, K.C. Xiao, Y.S. Choi, J.J. Vlassak, J. Appl. Phys. 114 (21) (2013), 214902. .
[22] D. Lee, G.-D. Sim, K. Zhao, J.J. Vlassak, Nano Lett. 15 (12) (2015) 8266–8270.
[23] E. Perim, D. Lee, Y.H. Liu, C. Toher, P. Gong, Y.L. Li, W.N. Simmons, O. Levy, J.J. Vlassak, J. Schroers, S. Curtarolo, Nat. Commun. 7 (2016).
[24] L. Stojanova, K. Russew, Mater. Sci. Eng. A 226 (1997) 483–486.
[25] Z. Altounian, T. Guo-hua, J.O. Strom-Olsen, J. Appl. Phys. 54 (6) (1983) 3111–3116.
[26] I. Kalay, M.J. Kramer, R.E. Napolitano, Metall. Mater. Trans. A 42A (5) (2011) 1144–1153.
[27] N. Mehta, K. Singh, N.S. Saxena, Physica B 403 (21−22) (2008) 3928–3931.
[28] M.D. Ediger, P. Harrowell, L. Yu, J. Chem. Phys. 128 (3) (2008), 034709. .
[29] C.V. Thompson, F. Spaepen, Acta Metall. 27 (12) (1979) 1855–1859.
[30] J.Q. Wang, N. Chen, P. Liu, Z. Wang, D.V. Louzguine-Luzgin, M.W. Chen, J.H. Perepezko, Acta Mater. 79 (2014) 30–36.
[31] K. Ohsaka, S.K. Chung, W.K. Rhim, Acta Mater. 46 (13) (1998) 4535–4542.
[32] K. Russew, L. Stojanova, S. Yankova, E. Fazakas, L.K. Varga, J. Phys. Conf. Ser. 144 (1) (2009) 012094.
[33] N.A. Mauro, M. Blodgett, M.L. Johnson, A.J. Vogt, K.F. Kelton, Nat. Commun. 5 (2014).
[34] W.L. Johnson, J.H. Na, M.D. Demetriou, Nat. Commun. 7 (2016).
[35] Z. Altounian, G.H. Tu, J.O. Stromolsen, J. Appl. Phys. 53 (7) (1982) 4755–4760.
[36] Y. Li, Q. Guo, J.A. Kalb, C.V. Thompson, Science 322 (5909) (2008) 1816–1819.
[37] H. Teichler, J. Non-Cryst. Solids 293-295 (2001) 339–344.
[38] H. Teichler, Defect Diffus. Forum 143-147 (1997) 717–722.
[39] M. Kluge, H.R. Schober, Defect and Diffusion Forum 194-199 (2001) 849–854.
[40] X.P. Tang, U. Geyer, R. Busch, W.L. Johnson, Y. Wu, Nature 402 (6758) (1999) 160–162.